Journal of Alloys and Compounds 523 (2012) 120–126

Contents lists available at SciVerse ScienceDirect

Journal of Alloys and Compounds

journal homepage: www.elsevier.com/locate/jallcom

Synthesis, characterization, and comparative gas-sensing properties of Fe_2O_3 prepared from Fe_3O_4 and Fe_3O_4-chitosan

Nguyen Duc Cuong [a,b,c], Tran Thai Hoa [b], Dinh Quang Khieu [b], Tran Dai Lam [d], Nguyen Duc Hoa [c], Nguyen Van Hieu [c,*]

[a] Faculty of Hospitality and Tourism, Hue University, 22 Lam Hoang, Vy Da Ward, Hue City, Viet Nam
[b] College of Sciences, Hue University, 77 Nguyen Hue, Phu Nhuan Ward, Hue City, Viet Nam
[c] International Training Institute for Materials Science (ITIMS), Hanoi University of Science and Technology (HUST), Hanoi, Viet Nam
[d] Institute of Materials Science, Vietnamese Academy of Science and Technology, Hanoi, Viet Nam

ARTICLE INFO

Article history:
Received 13 December 2011
Received in revised form 17 January 2012
Accepted 18 January 2012
Available online 27 January 2012

Keywords:
Fe_2O_3
Fe_3O_4
Gas sensor
Chitosan

ABSTRACT

In this paper, Fe_3O_4 and chitosan (CS)-coated Fe_3O_4 nanoparticles were synthesized via co-precipitation method and subsequent covalent binding of CS onto the surface for functionalization, respectively. Characterization of the crystal structures and morphologies of as-synthesized nanoparticles by X-ray diffraction, scanning electron microscopy, and transmission electron microscopy demonstrated that Fe_3O_4 had a cubic spinal structure with irregular shapes and average diameters of 10–20 nm. The surface states and magnetic properties of Fe_3O_4-CS nanoparticles were characterized by Fourier transform infrared spectra and vibrating sample magnetometry. Results showed that Fe_3O_4-CS nanoparticles possessed super-paramagnetic properties, with saturated magnetization up to 60 emu/g. In addition, Fe_3O_4 and CS-coated Fe_3O_4 nanoparticles were used in the fabrication of α-Fe_2O_3 based gas sensors. Gas sensing measurements revealed that the α-Fe_2O_3 gas sensor prepared from Fe_3O_4-CS had a better response to H_2, CO, C_2H_5OH, and NH_3 compared with the device prepared from pristine Fe_3O_4. Furthermore, the α-Fe_2O_3 sensor prepared from Fe_3O_4-CS nanoparticles exhibited the highest response to CO among the test gases, suggesting that it has great potential for practical applications in environmental monitoring.

1. Introduction

In recent decades, functional metal oxide nanocrystals such as Fe_3O_4 and Fe_2O_3 have been extensively investigated due to their outstanding properties and suitability for diverse applications [1]. Among the metal oxides, iron oxide nanoparticles (NPs) have been of great interest not only in terms of their fundamental properties caused by their multivalent oxidation states, abundant polymorphism, and mutual polymorphous changes in nanophases, but also in the field of technological applications such as high density magnetic recording media, sensors, catalysts, and clinical uses [2]. Iron (III) oxide (Fe_2O_3) materials have four phases: α-Fe_2O_3 (hematite); β-Fe_2O_3; γ-Fe_2O_3 (maghemite); and ε-Fe_2O_3 [3]. The nanocrystals of magnetic γ-Fe_2O_3 have been applied in information storage, magnetic refrigeration, bioprocessing, controlled drug delivery, and ferrofluids [4–6], while α-Fe_2O_3 is environmentally friendly and has been used for gas sensor, lithium ion battery, catalyst and pigment applications [7–9].

Aside from ferric oxide, magnetite (Fe_3O_4), an important kind of magnetic material with a cubic inverse spinal structure, has also been received increasing attention because of its wide use in magnetic recording, ferrofluid, catalyst, magnetic resonance imaging (MRI), bio-separation, drug targeting, and hyperthermia [10–12]. For biomedical applications, Fe_3O_4 NPs are often treated with surface modification in order to increase their chemical stability and improve their biocompatibility. A variety of materials have been investigated for the modification of Fe_3O_4 NPs: precious metals [13], silica [14], carbon [15], biopolymers [16–18], and CS. Among these materials, CS is a partially acetylated glucosamine biopolymer with many useful features such as hydrophilicity, biocompatibility, and biodegradability. In addition, the amino groups of CS can also be used for further functionalization of specific components, such as various drugs, specific binding sites, and other functional groups. Thus, CS is a suitable polymer for the modification of Fe_3O_4 NPs [19–21].

In terms of the performance of gas sensing applications, nanomaterials are clearly superior due to their high specific surface area and controllable structures. A large specific surface area is critical for reactive gas adsorption and results in high response magnitude and sensitivity. Nanostructured materials often possess enhanced reactivity because of a strained surface lattice and/or

* Corresponding author at: No. 1 Dai Co Viet, Hanoi, Vietnam.
Tel.: +84 4 38680787; fax: +84 4 38692963.
E-mail address: hieu@itims.edu.vn (N. Van Hieu).

0925-8388/$ – see front matter © 2012 Elsevier B.V. All rights reserved.
doi:10.1016/j.jallcom.2012.01.117

increased prevalence of step, edge, corner, and terrace sites. Such activities further enhance response and potentially decrease operational temperature. In turn, operation at lower temperatures saves power, extends operating lifetime, and maintains reproducibility by preventing sintering-induced grain growth. Furthermore, lower operational temperature, combined with structure control, can also advantageously improve selectivity [22]. Nanostructured iron oxides have received increasing attention in the field of gas sensors in recent years [23]. The iron oxides exhibit excellent surface reactivity with temperature-dependent surface morphology. They also exhibit remarkable catalytic properties in oxidative reactions due to the high oxygen ion mobility at the material surface and are thus highly promising for sensor development [24].

In the present study, we introduced the synthesis of Fe_3O_4 NPs through a co-precipitation process and subsequently modified the synthesized NPs with CS. The adsorption and modification of CS onto the surface of Fe_3O_4 NPs were investigated to optimize the colloidal stability of Fe_3O_4 NPs. Structures and magnetic properties of synthesized NPs were investigated using advanced techniques. Furthermore, synthesized Fe_3O_4 and Fe_3O_4-CS NPs were transformed into α-Fe_2O_3 phase by heat treatment in air atmosphere at high temperature for gas sensing applications. Effects of Fe_3O_4 and Fe_3O_4-CS NPs on the sensing performances of prepared α-Fe_2O_3 sensors for the detection of H_2, CO, C_2H_5OH, and NH_3 gases were evaluated and compared.

2. Experimental

2.1. Materials

All reagents were of analytical grade and used without further purification. Ferric chloride hexahydrate ($FeCl_3{\cdot}6H_2O$, Merck), ferrous chloride tetrahydrate ($FeCl_2{\cdot}4H_2O$, Merck), and CS (Quangzi, China) were used as iron and polymer-stabilizer sources, respectively. Hydrochloric acid (HCl, Quangzi, China) and sodium hydroxide (NaOH, Quangzi, China) were used to adjust the pH of solutions for co-precipitation of Fe_3O_4 NPs.

2.2. Preparation of Fe_3O_4 and Fe_3O_4-CS nanoparticles

Fe_3O_4 NPs were synthesized through the co-precipitation method using ferric chloride and ferrous chloride as iron sources. In a typical synthesis, ferric chloride (2 mmol) and ferrous chloride (1 mmol) were dissolved in 100 ml HCl (pH 2) to obtain a homogenous solution. Chemical precipitation was achieved by the slow addition of NaOH solution (0–1 mol/l) during vigorous stirring for 30 min at 80 °C. Precipitated products were recovered through filtering, washing, and drying at 60 °C. In order to modify Fe_3O_4 NPs, the collected powder was dispersed in distilled water (1 g/100 ml) and a CS solution (1 g/100 ml) was slowly added with vigorous stirring at 50 °C for 30 min. The modified Fe_3O_4-CS NPs were recovered through filtering, washing, and drying at room temperature.

X-ray diffraction (XRD) was performed to identify the crystal structures of Fe_3O_4, Fe_3O_4-CS, and -Fe_2O_3 (D8 Advance, Brucker, Germany). Morphologies were studied by transmission electron microscopy (TEM, Model JEOLE-3432, Japan). Magnetic properties were analyzed using a vibrating sample magnetometer (VSM). Infrared (IR) spectra were recorded using a Nicolet 6700 FTIR Spectrometer.

2.3. Gas sensing measurements

To characterize gas sensing properties, synthesized Fe_3O_4 and Fe_3O_4-CS NPs were dispersed in ethanol and deposited on a pre-fabricated interdigitated electrode substrate using a micropipette. Fe_3O_4 and Fe_3O_4-CS films were then heat-treated in normal atmospheric conditions at 600 °C for 5 h to transform Fe_3O_4 into the α-Fe_2O_3 phase.

The gas sensing properties of α-Fe_2O_3 NPs were studied by testing all sensors with H_2 (25–500 ppm), CO (10–100 ppm), C_2H_5OH (50–500 ppm), and NH_3 (50–5000 ppm) at different temperatures (300–400 °C) using a homemade set up with high speed switching gas flow (from/to air to/from balance gas). Balance gases (0.1% in air) were purchased from Air Liquid Group (Singapore). Flow through of the system was employed with a constant flow-rate of 200 sccm. Detailed information about the gas testing system is presented in [25].

3. Results and discussion

The crystal structures and phase transformation of Fe_3O_4, Fe_3O_4-CS, and Fe_2O_3 NPs revealed by XRD are presented in Fig. 1a and b. XRD patterns of Fe_3O_4 and Fe_3O_4-CS NPs exhibited typical Fe_3O_4 cubic structure, where all diffraction peaks are well indexed to the (2 2 0), (3 1 1), (4 0 0), (4 2 2), (5 1 1), and (4 4 0) planes (JCPDS No. 19-0629). The weaker diffraction lines of Fe_3O_4-CS NPs indicate that the Fe_3O_4 particles were successfully coated by amorphous CS. However, CS coating did not change the crystal structure of Fe_3O_4. The average crystal size of synthesized NPs was calculated using the Debye–Scherrer equation:

$$d = \frac{k\lambda}{\beta\cos\theta} \quad (1')$$

where d is the average crystal size of particles, k is the Debye–Scherrer constant (0.89), λ is the X-ray wavelength (0.15406 nm), β is the line broadening in a radian obtained from the full width at half maximum, and θ is the Bragg angle. The average crystal size of uncoated Fe_3O_4 and CS-coated Fe_3O_4 is 15.4 and 13.2 nm, respectively.

The crystal structure of the as-synthesized α-Fe_2O_3 is shown in Fig. 1b. The XRD pattern indicates that all the peaks could be perfectly indexed to a pure rhombohedral crystalline phase of α-Fe_2O_3, according to JCPDS Card No. 81-2810. No impurities and peaks of other phases were detected, indicating that the products were quite purity.

TEM micrographs of pure Fe_3O_4 and CS-coated Fe_3O_4 NPs (Fig. 2) demonstrate that their diameters were in the range of 10–20 nm. Pure Fe_3O_4 NPs were quite agglomerated, while the morphology of CS-coated magnetite NPs exhibited highly dispersed particles. These results are consistent with those obtained by size calculation from XRD. FE-SEM images of Fe_3O_4 and CS-coated Fe_3O_4 powder were also recorded, but differences in their morphologies were difficult to find (Fig. 2c and d). α-Fe_2O_3 NPs obtained from the heat-treatment of Fe_3O_4 and CS-coated Fe_3O_4

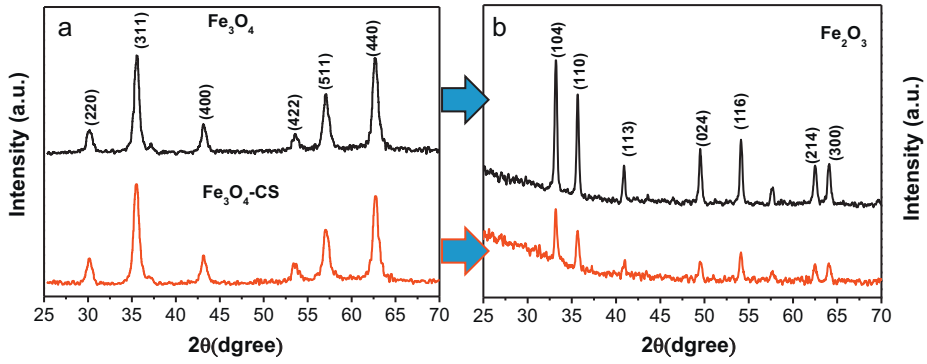

Fig. 1. XRD pattern of Fe_3O_4 and chitosan-coated Fe_3O_4 (a) and Fe_2O_3 obtained from heat treatment of Fe_3O_4 and chitosan-coated Fe_3O_4 (b).

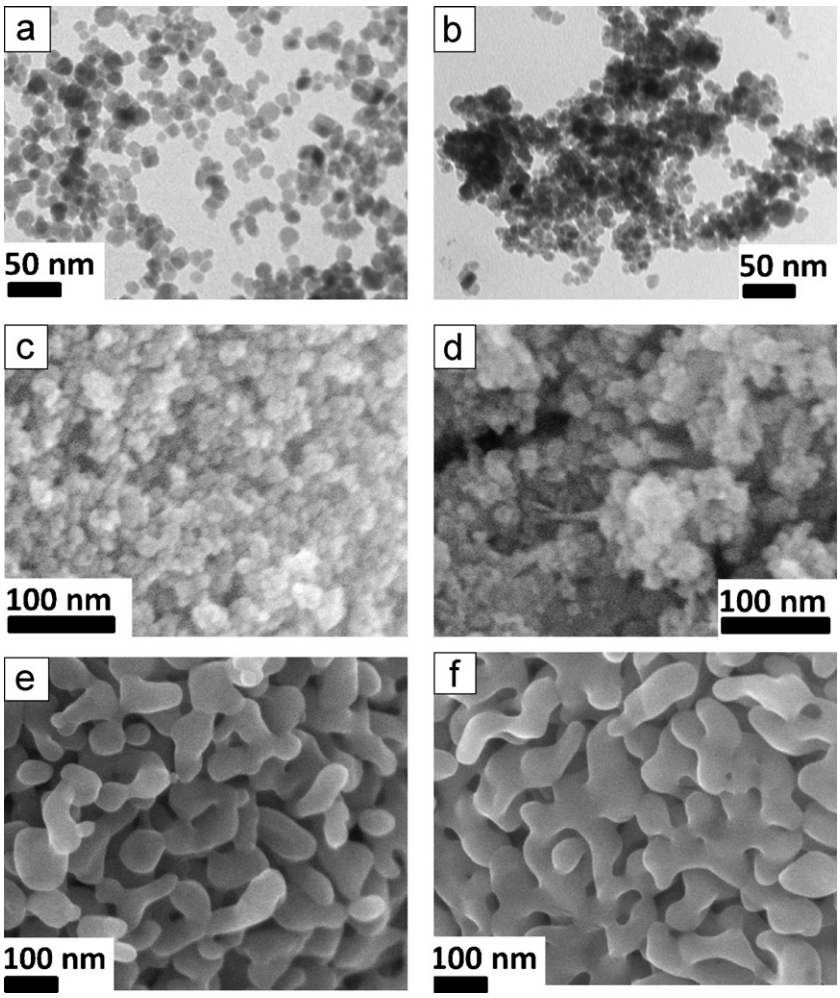

Fig. 2. TEM images of chitosan-coated Fe_3O_4 (a) and Fe_3O_4 (b); FE-SEM images of chitosan-coated Fe_3O_4 powder (c), Fe_3O_4 powder (d), and Fe_2O_3-obtained from chitosan-coated Fe_3O_4 (e) and Fe_3O_4 (f).

samples were relatively more porous (Fig. 3e and f), which could have implications in gas-sensing performance.

The magnetic hysteresis curves of pristine Fe_3O_4 and Fe_3O_4-CS NPs are shown in Fig. 3. No coercivity or remanence could be observed for the two samples, suggesting that Fe_3O_4 NPs have superparamagnetic properties. This observation can be ascribed to the small size of NPs, which is less than the superparamagnetic critical size (25 nm) [15]. The saturation magnetization of pristine Fe_3O_4 NPs was relatively high (76.68 emu/g), indicating good crystal structure. In contrast, Fe_3O_4-CS NPs had a lower saturation magnetization (60 emu/g) due to the large amount of diamagnetic CS present.

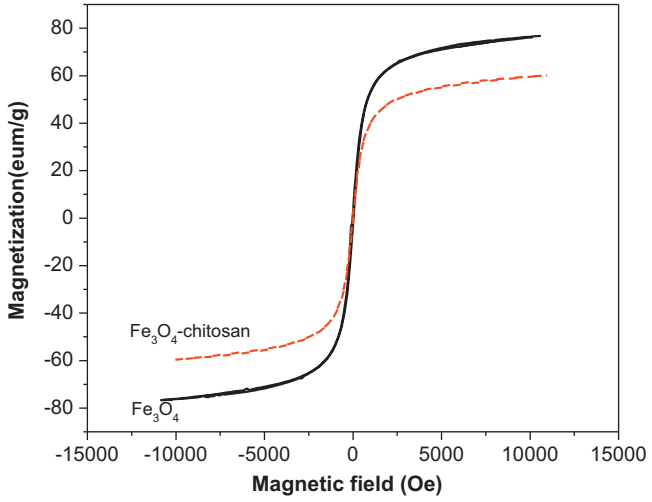

Fig. 3. Magnetization versus applied field (H) isotherms for chitosan-coated Fe_3O_4 and Fe_3O_4 nanoparticles (a); TGA curves of chitosan-coated Fe_3O_4 nanoparticles (b).

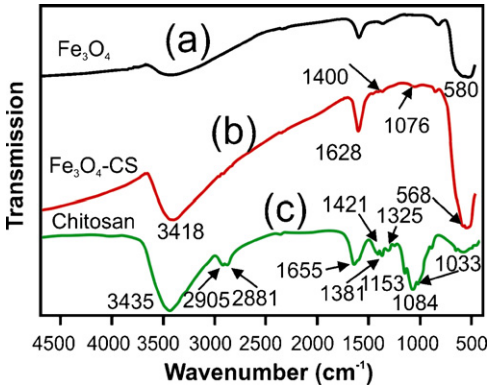

Fig. 4. FT-IR of spectra of pristine Fe_3O_4 NPs (a), chitosan-coated Fe_3O_4-chitosan (b), and chitosan (c).

Fig. 4 shows the FT-IR of spectra of pristine Fe_3O_4 NPs (a), Fe_3O_4-CS (b), and CS (c). The characteristic peaks of Fe_3O_4 at 580 and 568 cm^{-1} could be observed in both (b) and (c), which identifies these NPs as Fe_3O_4. The IR spectrum of CS was characterized using the following absorption bands: (C—H) of backbone polymer appearing at 2905 and 2881 cm^{-1}; (C_3—O) of primary alcoholic group at 1421 cm^{-1}; (C—O), amide I at 1084 and 1033 cm^{-1}; and (N—H) and amide II of primary admine at 3400 and 1655 cm^{-1}. Compared with the IR spectra of (a), (b), and (c) samples, the presence of CS minimally shifted the vibration of Fe_3O_4. The band shift of Fe—O stretching (from 580 to 568 cm^{-1}) and of N—H bending vibration from 1655 to 1628 cm^{-1} are the most significant, indicating that iron ions possibly bind to the NH_2 group of CS. Electrostatic interaction between the negatively charged Fe_3O_4 surface and the positively protonated CS also contributes to the IR change. Our findings suggest that Fe_3O_4 NPs and CS became integrated into Fe_3O_4-CS NPs.

We systematically investigated the gas-sensing performance of Fe_2O_3 sensors prepared from heat-treatment of Fe_3O_4 and CS-coated Fe_3O_4 NPs, hereafter referred to as "Fe_2O_3 sensor" and "Fe_2O_3-CS sensors". Sensors were tested with various gases (H_2, CO, C_2H_5OH, and NH_3) at different gas concentrations and working temperatures. The sensing mechanism of the Fe_2O_3 NP-based gas sensors to these reducing gases can be explained by the depletion region. During the gas-sensing measurement, the oxygen in the air captured the electrons from the Fe_2O_3 crystal and ion-adsorbed (O_2^-, O^- and O^{2-}) on the surface of the sensing layer; this phenomenon resulted in the formation of the electron-depletion region [22]. Upon exposure to H_2, CO, C_2H_5OH, and NH_3, these molecules interacted with the pre-adsorbed oxygen and released electrons, according to the equations:

$$H_2 + O^-(ads) \leftrightarrow H_2O + e^- \quad (1)$$

$$CO + O^-(ads) \leftrightarrow CO_2 + e^- \quad (2)$$

$$C_2H_5OH + 6O^-(ads) \leftrightarrow 2CO_2 + 3H_2O + 6e^- \quad (3)$$

$$2NH_3 + 7O^-(ads) \leftrightarrow 2NO_2 + 3H_2O + 7e^- \quad (4)$$

The release of free electrons increased the total carrier and reduced the electron-depletion region, resulting in a decrease in sensor resistance (e.g. sensors response, R_{air}/R_{gas} increases). After the analytic gas flow was discontinued, the adsorption of oxygen molecules onto the surface of the sensing layer returned the sensor resistance to the initial value.

Fig. 5 presents the H_2 sensing characteristics of Fe_2O_3 and Fe_2O_3-CS sensors. The typical responses of these sensors to 500 ppm H_2 at 300, 350, and 400 °C (Fig. 5a and b) demonstrate that the optimum operating temperature for both sensors is 350 °C. For H_2 sensing at the optimum operating temperature (Fig. 5c and d), the Fe_2O_3-CS sensor demonstrated a better sensing performance than the Fe_2O_3 sensor. Sensor response as a function of H_2 gas concentration (Fig. 5d) demonstrated that the response of the Fe_2O_3-CS sensor is significant enhanced with H_2 gas concentration. H_2 sensors have been extensively investigated [26], although studies on H_2 sensors based on Fe_2O_3 are few. The H_2 sensing response in the present work was relatively better than that of the previously reported Fe_2O_3 thin film [27] and Zn-doped Fe_2O_3 sensor [28].

The Fe_2O_3 and Fe_2O_3-CS sensors were also tested with CO gas applying the same procedure used for H_2 gas testing (Fig. 6). Responses of the two sensors slightly varied at the operating temperature range of 300–400 °C. The optimum operating temperature was 350 °C, which concurs with the results of the H_2 gas test. Testing with different CO gas concentrations (Fig. 6c and d) revealed that the Fe_2O_3-CS sensor had better performance than the Fe_2O_3 sensor. In contrast to the results of the H_2 gas test, the response of the two sensors differed at low CO gas concentration (10 ppm). The CO gas sensing properties of Fe_2O_3-based sensors have not been investigated extensively. The Fe_2O_3-CS sensor in the present work showed much better CO gas sensing performance compared with the few works reported previously [29,30].

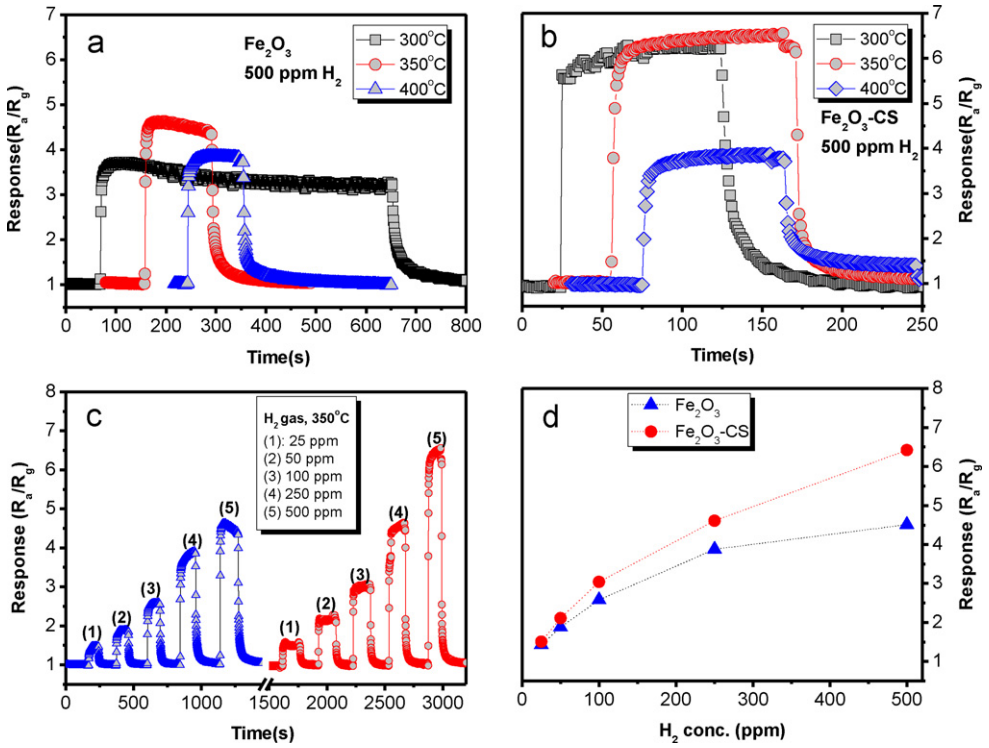

Fig. 5. H_2 sensing characteristics of α-Fe_2O_3; transient response of the Fe_2O_3 sensors prepared from Fe_3O_4 (a) and chitosan-coated Fe_3O_4 (b); the response of the both sensors to various concentrations at optimum operating temperature (c), and sensor response as a function of gas concentration (d).

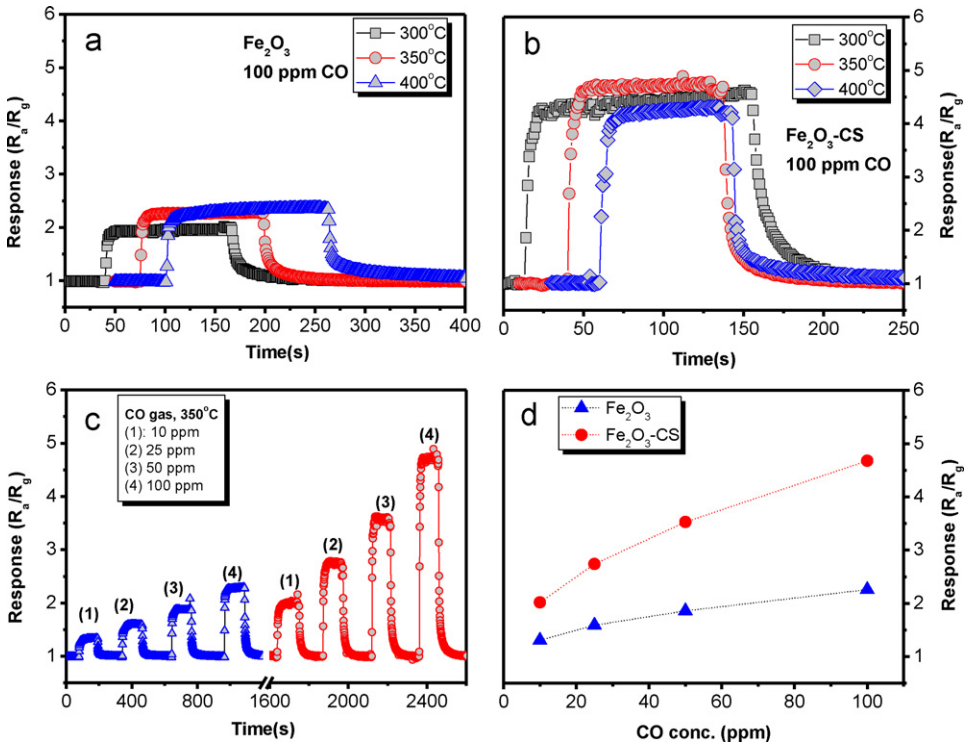

Fig. 6. CO sensing characteristics of α-Fe_2O_3; transient response of the Fe_2O_3 sensors prepared from Fe_3O_4 (a) and chitosan-coated Fe_3O_4 (b); the response of the both sensors to various concentrations at optimum operating temperature (c), and sensor response as a function of gas concentration (d).

The ethanol sensing characteristics of Fe_2O_3 and Fe_2O_3-CS sensors were also investigated. Fig. 7a and b shows the transient response of the two sensors to 500 ppm C_2H_5OH at different operating temperatures (300, 350, and 450 °C). The optimum operating temperature of the Fe_2O_3 sensor is 350 °C, whereas the Fe_2O_3-CS sensor exhibited only slight differences in the response at the operating temperature range (300–400 °C). Testing of the sensors using different ethanol gas concentrations at 350 °C showed only slight differences in sensing performance (Fig. 7c). Compared with the H_2 and CO sensing behaviors, higher ethanol gas concentration

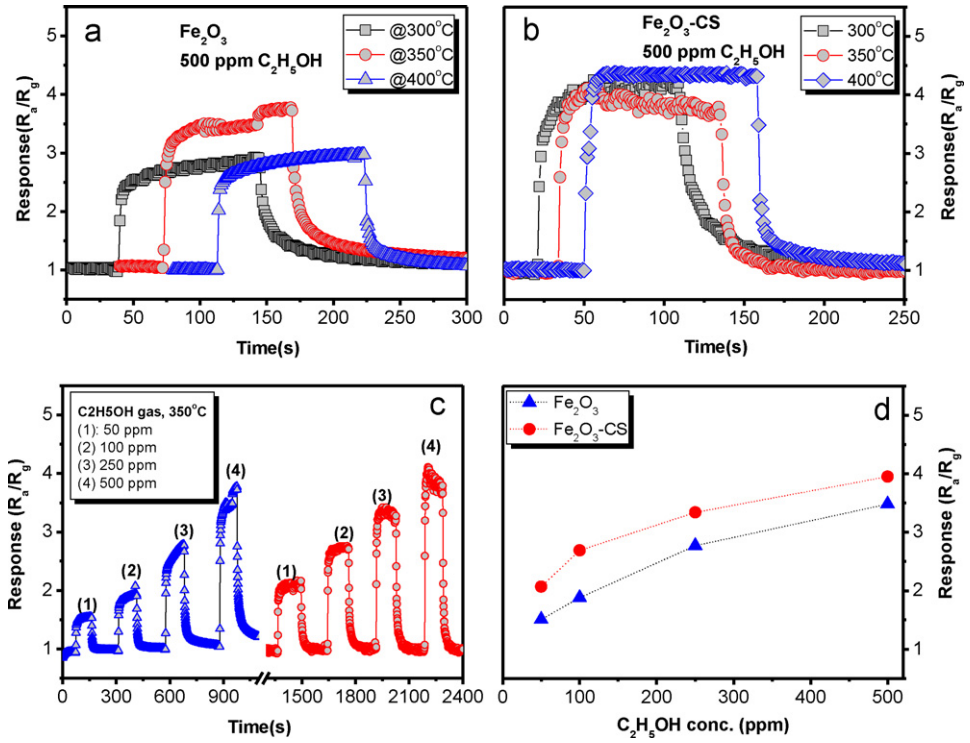

Fig. 7. C_2H_5OH sensing characteristics of α-Fe_2O_3; transient response of the Fe_2O_3 sensors prepared from Fe_3O_4 (a) and chitosan-coated Fe_3O_4 (b); the response of the both sensors to various concentrations at optimum operating temperature (c), and sensor response as a function of gas concentration (d).

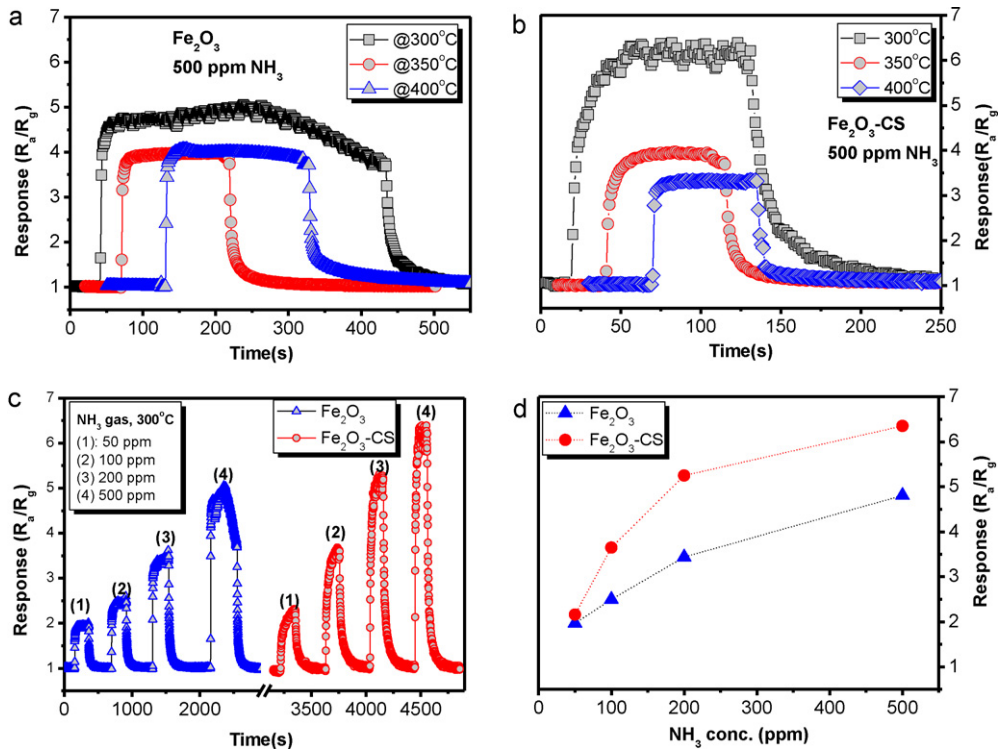

Fig. 8. NH_3 sensing characteristics of α-Fe_2O_3; transient response of the Fe_2O_3 sensors prepared from Fe_3O_4 (a) and chitosan-coated Fe_3O_4 (b); the response of the both sensors to various concentrations at optimum operating temperature (c), and sensor response as a function of gas concentration (d).

did not lead to significant changes in response of the two sensors (Fig. 7d). Further investigation of the underlying mechanism is needed. We speculate that the relatively larger molecules of ethanol gas allow them to dissociate and react with the surface oxygen of the Fe_2O_3 film, so that pore-size distribution does not influence sensor responses. A narrow particle-size distribution results in a narrow pore-size distribution. Different studies have reported ethanol gas sensing properties [29–33]. Compared with the present study, better responses to ethanol gas of α-Fe_2O_3-based sensors with other additive materials have been reported.

The NH_3 gas detection ability of α-Fe_2O_3-based sensors has not been fully explored [27,34]. The transient responses of α-Fe_2O_3 and α-Fe_2O_3-CS sensors to 500 ppm NH_3 at different operating temperatures (300, 350, and 400 °C) are shown in Fig. 8a and b. Both sensors have an optimum operating temperature of 300 °C, which was lower than that found in the H_2, CO, and ethanol tests. Both sensors were then tested with different NH_3 gas concentrations at 300 °C (Fig. 8c). The α-Fe_2O_3-CS sensor exhibited better performance than the α-Fe_2O_3 sensor. The response of both sensors represented as a function of NH_3 gas concentration is shown in Fig. 8d. The same sensing behavior was also observed with H_2 and CO gases, where the response of the α-Fe_2O_3-CS sensor to NH_3 gas was significantly higher than that of the α-Fe_2O_3 sensor at high gas concentrations.

For an overall comparison of the responses to H_2, CO, C_2H_5OH, and NH_3 gases, the ratio between the response of α-Fe_2O_3-CS sensor to that of α-Fe_2O_3 sensor ($S(\alpha\text{-}Fe_2O_3\text{-CS})/S(\alpha\text{-}Fe_2O_3)$) was plotted for 100 ppm of each gas at different operating temperatures (Fig. 9). The use of CS for coating of Fe_3O_4 NPs during the preparation of the α-Fe_2O_3 sensor enhanced sensor response, and the greatest response improvement for all tested gases was observed at an operating temperature of 300 °C. The response of α-Fe_2O_3-CS sensor to CO was the strongest enhancement among the other gases (Fig. 9), and additional studies are needed to explain this observation. We speculate that the kinetic diameter of the CO gas molecule

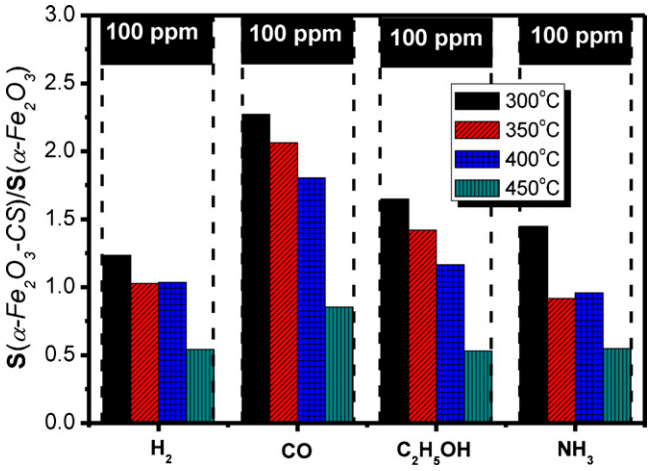

Fig. 9. The ratio between the response of α-Fe_2O_3-CS sensor to that of α-Fe_2O_3 sensor for 100 ppm H_2, CO, C_2H_5OH, and NH_3 gases at different operating temperatures.

is more comparable with the pore-size distribution of α-Fe_2O_3 NPs. The narrow pore-size distribution due to the homogenous particle-size can lead to greater enhancement of the gas diffusion ability of the CO gas molecule compared with other gas molecules. Consequently, sensor response can be enhanced by a narrower pore-size distribution. This question is outside the scope of the present study and further studies are in progress to better investigate the behavior of both sensors. Further investigation may lead to the development of α-Fe_2O_3-based sensors for the detection of various gases.

4. Conclusion

In this study, we synthesized Fe_3O_4 NPs through co-precipitation and demonstrated the process of CS-coating of Fe_3O_4.

The morphology, microstructure, and magnetic properties of Fe_3O_4 and CS-coated Fe_3O_4 were investigated and compared. The performance of α-Fe_2O_3 sensors obtained from Fe_3O_4 and CS-coated Fe_3O_4 were compared at different operating temperatures and to various gases (e.g. H_2, CO, C_2H_5OH, and NH_3). The α-Fe_2O_3 sensor prepared from CS-coated Fe_3O_4 NPs showed better performance than that prepared from naked Fe_3O_4 NPs. In comparison with all tested gases, the α-Fe_2O_3 based sensors exhibited relatively good response to CO gas.

Acknowledgment

This work was financially supported by the Application-Oriented Basic Research Program (2009–2012, Code: 05/09/HĐ-DTĐL).

References

[1] W.-H. Yang, C.-F. Lee, H.Y. Tang, D.-B. Shieh, C.-S. Yeh, J. Phys. Chem. B 110 (2006) 14087–14091.
[2] K. Woo, J. Hong, S. Choi, H.-W. Lee, J.-P. Ahn, C.S. Kim, S.W. Lee, Chem. Mater. 16 (2004) 2814–2818.
[3] R.M. Cornell, U. Schwertmann, The Iron Oxide: Structure, Properties, Reaction, Occurrences and Users, Wiley-VCH, Germany, 2003, pp. 29–32.
[4] Y.-J. Lee, K.-W. Jun, J.-Y. Park, H.S. Potdar, R.C. Chikate, J. Ind. Eng. Chem. 14 (2008) 38–44.
[5] I. Ray, S. Chakraborty, A. Chowdhury, S. Majumdar, A. Prakash, R. Pyare, A. Sen, Sens. Actuators B 130 (2008) 882–888.
[6] S. Radhakrishnan, C. Saujanya, P. Sonar, I.K. Gopalkrishnan, J.V. Yakhmi, Polyhedron 20 (2001) 1489–1494.
[7] T.-J. Park, S.S. Wong, Chem. Mater. 18 (2006) 5289–5295.
[8] J.S. Chen, T. Zhu, X.H. Yang, H.G. Yang, X.W. Lou, J. Am. Chem. Soc. 132 (2010) 13162–13164.
[9] J. Gu, S. Li, E. Wang, Q. Li, G. Sun, R. Xu, H. Zhang, J. Solid State Chem. 182 (2009) 1265–1272.
[10] S. Laurent, D. Forge, M. Port, A. Roch, C. Robic, L.V. Elst, R.N. Muller, Chem. Rev. 108 (2008) 2064–2110.
[11] S. Wei, Y. Zhu, Y. Zhang, J. Xu, React. Funct. Polym. 66 (2006) 1272–1277.
[12] Y.F. Shen, J. Tang, Z.H. Nie, Y.D. Wang, Y. Renc, L. Zuo, Sep. Purif. Technol. 68 (2009) 312–319.
[13] L.Y. Wang, H.Y. Park, S.I.I. Lim, M.J. Schadt, D. Mott, J. Luo, X. Wang, C.J. Zhong, J. Mater. Chem. 18 (2008) 2629–2635.
[14] R.-Y. Hong, J.-H. Li, S.-Z. Zhang, H.-Z. Li, Y. Zheng, J.-M. Ding, D.-G. Wei, Appl. Surf. Sci. 255 (2009) 3485–3492.
[15] L.Q. Xu, W.Q. Zhang, Y.W. Ding, Y.Y. Peng, S.Y. Zhang, W.C. Yu, Y.T. Qian, J. Phys. Chem. B 108 (2004) 10859–10862.
[16] X.Q. Xu, H. Shen, J.R. Xu, M.Q. Xie, X.J. Li, Appl. Surf. Sci. 253 (2006) 2158–2164.
[17] H.V. Tran, L.D. Tran, T.N. Nguyen, Mater. Sci. Eng. C 30 (2010) 304–310.
[18] L.D. Tran, B.H. Nguyen, N.V. Hieu, H.V. Tran, H.L. Nguyen, P.X. Nguyen, Mater. Sci. Eng. C 31 (2011) 477–485.
[19] B. Feng, R.Y. Hong, Y.J. Wu, G.H. Liu, L.H. Zhong, Y. Zheng, J.M. Ding, D.G. Wei, J. Alloys Compd. 473 (2009) 356–362.
[20] K. Donadel, M.D.V. Felisberto, V.T. Favere, M. Rigoni, N.J. Batistela, M.C.M. Laranjeira, Mater. Sci. Eng. C 28 (2008) 509–514.
[21] D.L. Zhao, X.X. Wang, X.W. Zeng, Q.S. Xia, J.T. Tang, J. Alloys Compd. 477 (2009) 739–743.
[22] R.L.V. Wal, G.W. Hunter, J.C. Xu, M.J. Kulis, G.M. Berger, T.M. Ticich, Sens. Actuators B 138 (2009) 113–119.
[23] N. Hongsith, E. Wongrat, T. Kerdcharoen, S. Choopun, Sens. Actuators B 144 (2010) 67–72.
[24] F. Zhang, H. Yang, X. Xie, L. Li, L. Zhang, J. Yu, H. Zhao, B. Liu, Sens. Actuators B 141 (2009) 381–389.
[25] L.V. Thong, L.T.N. Loan, N.V. Hieu, Sens. Actuators B 150 (2010) 112–119.
[26] T. Hubert, L. Boon-Brett, G. Black, U. Banach, Sens. Actuators B 20 (2011) 329–352.
[27] K. Hara, A. Nishida, Sens. Actuators B 20 (1994) 181–186.
[28] T. Kim, B. Guo, J. Ind. Eng. Chem. 177 (2011) 158–164.
[29] Q. Hao, S. Liu, X. Yin, Y. Wang, Q. Li, T. wang, Solid State Sci. 12 (2010) 2125–2129.
[30] G. Neri, A. Bonavita, S. Galvagno, C. Pace, N. Donato, J. Mater. Sci.: Mater. Electron. 13 (2002) 561–565.
[31] L. Huo, Q. Li, H. Zhao, L. Yu, S. Gao, J. Zhao, Sens. Actuators B 107 (2005) 915–920.
[32] O.K. Tan, W. Cao, W. Zhu, J.W. Chai, J.S. Pan, Sens. Actuators B 93 (2003) 396–401.
[33] O.K. Tan, W. Zhu, Q. Yan, L.B. Kong, Sens. Actuators B 65 (2000) 361–365.
[34] D.R. Patil, L.A. Patil, Sensors 70 (2006) 661–670.